Neuroscience 231 (2013) 195–205

REDUCED SEIZURE THRESHOLD AND ALTERED NETWORK OSCILLATORY PROPERTIES IN A MOUSE MODEL OF RETT SYNDROME

F. MCLEOD,[a] R. GANLEY,[a] L. WILLIAMS,[a] J. SELFRIDGE,[b] A. BIRD[b] AND S. R. COBB[a]*

[a] *Institute for Neuroscience and Psychology, College of Medical, Veterinary and Life Sciences, University of Glasgow, Glasgow G12 8QQ, UK*

[b] *Wellcome Trust Centre for Cell Biology, Edinburgh University, The King's Buildings, Edinburgh EH9 3JR, UK*

Abstract—Rett syndrome (RTT) is a disorder with a pronounced neurological phenotype and is caused mainly by mutations in the X-linked gene *MECP2.* A common feature of RTT is an abnormal electroencephalography and a propensity for seizures. In the current study we aimed to assess brain network excitability and seizure propensity in a mouse model of RTT. Mice in which *Mecp2* expression was silenced (*Mecp2*$^{stop/y}$) showed a higher seizure score (mean = 6 ± 0.8 compared to 4 ± 0.2 in wild-type [WT]) and more rapid seizure onset (median onset = 10 min in *Mecp2*$^{stop/y}$ and 32 min in WT) when challenged with the convulsant drug kainic acid (25 mg/kg). Hippocampal slices from *Mecp2*$^{stop/y}$ brain displayed no spontaneous field potential activities under control conditions but showed higher power gamma frequency field potential oscillations compared to WT in response to kainic acid (400 nM) *in vitro*. Brain slices challenged with the $GABA_A$-receptor antagonist bicuculline (0.1–10 μM) and the potassium channel blocker 4-aminopyridine (1–50 μM) also revealed differences between genotypes with hippocampal circuits from *Mecp2*$^{stop/y}$ mouse slices showing enhanced epileptiform burst duration and frequency. In contrast to these network level findings, single cell analysis of pyramidal cells by whole-cell patch clamp recording revealed no detectable differences in synaptic or biophysical properties between methyl-CpG-binding protein 2 (MeCP2)-containing and MeCP2-deficient neurons. These data support the proposal that loss of MeCP2 alters network level excitability in the brain to promote epileptogenesis.

Key words: MECP2, Rett Syndrome, epilepsy, gamma oscillations, excitability, network.

INTRODUCTION

Rett syndrome (RTT), traditionally considered a neurodevelopmental disorder, mainly affects girls and is principally due to mutations in the x-linked gene methyl-CpG-binding protein 2 (*MECP2*) (Amir et al., 1999; Neul et al., 2010; Gadalla et al., 2011). The age of onset can vary with characteristic symptoms including loss of speech, reduced head growth, stereotypic hand movements, motor dysfunction and autistic-like features (Chahrour and Zoghbi, 2007; Neul et al., 2010). The development of epilepsy in ~50–80% of RTT patients is another prominent phenotype (Hagberg et al., 2002; Glaze et al., 2010) with diverse seizure types ranging from complex partial to myoclonic seizures (Steffenburg et al., 2001; Kim et al., 2012). Epilepsies are thus common in RTT and have an age-related onset but with the severity of seizures appearing to fall in late adolescence (Steffenburg et al., 2001). Some authors report no significant clinical difference in seizures between patient genotypes (Cardoza et al., 2011) but a recent large scale study suggests that seizures may indeed vary by mutation type with T158M (74%) and R106W (78%) mutations being most frequently associated with epilepsy (Glaze et al., 2010). The occurrence of seizures is also associated with a greater overall clinical severity including impaired ambulation and communication. Abnormal electroencephalography (EEG) recordings are commonly detected in RTT patients including giant evoked somatosensory potentials (cortical hyperexcitability), epileptiform abnormalities and the occurrence of rhythmic slow theta activity (Glaze, 2005). Whilst the EEG is invariably abnormal at some stage, there is no characteristic or diagnostic EEG pattern for RTT (Glaze, 2005).

Whilst the majority (> 95%) of classical RTT cases are due to mutations in the gene methyl-CpG-binding protein 2 (*MECP2*), the underlying function of MeCP2 protein and its regulation remain unclear (Gadalla et al., 2011; Guy et al., 2011). Many lines of mice have been developed in which *Mecp2* has been deleted, silenced or mutated to mimic major human mutations and these mouse lines replicate many of the features observed in RTT patients (Chen et al., 2001; Guy et al., 2001, 2007; Shahbazian et al., 2002; Goffin et al., 2012) and provide valuable tools for investigating MeCP2-related function/dysfunctions. EEG recordings reveal *Mecp2*-null mice to display abnormal spontaneous rhythmic discharges of 6–9 Hz in the somatosensory cortex during wakefulness and altered theta frequency hippocampal rhythms

*Corresponding author. Tel: +44-(0)141-330-2914.
E-mail address: Stuart.Cobb@glasgow.ac.uk (S. R. Cobb).

Abbreviations: 4-AP, 4-aminopyridine; ACSF, artificial cerebrospinal fluid; ANOVA, analysis of variance; EEG, electroencephalography; EGTA, ethylene glycol tetraacetic acid; fEPSPs, field excitatory postsynaptic potentials; HEPES, hydroxyethyl piperazineethanesulfonic acid; KA, kainic acid; MANOVA, multivariate analysis of variance; MeCP2, *Mecp2*, *MECP2*, methyl-CpG-binding protein 2; RTT, Rett syndrome; SEM, standard error of the mean; WT, wild-type.

0306-4522/12 $36.00
http://dx.doi.org/10.1016/j.neuroscience.2012.11.058

(D'Cruz et al., 2010) with some similarities to those observed in RTT patients. In addition to background rhythms, recent studies have shown alterations in the amplitude and latency of event-related potentials (ERPs), brain activations that occur during certain behavioural tasks, in *Mecp2*-null mice suggesting alterations in the strength and timing of cognitive processes (Goffin et al., 2012). This study also reported an increased power of high gamma frequency (70–140 Hz) EEG in *Mecp2*-null mice compared to controls, an activity that can be observed in the EEG before and during seizures and perhaps indicative of a hyper-excitability phenotype (Goffin et al., 2012). Spontaneous myoclonic seizures have also been reported in mice expressing a truncated form of MeCP2 (Shahbazian et al., 2002).

Cellular level studies have indicated alterations in the balance between synaptic inhibition and excitation in cortical/hippocampal circuits of the *Mecp2*-null mouse (Dani et al., 2005). Features reported include reduced excitatory synaptic function (Dani et al., 2005; Asaka et al., 2006; Nelson et al., 2006), reduced synaptic plasticity (Asaka et al., 2006; Guy et al., 2007; Weng et al., 2011), altered connectivity in terms of excitatory synapses/spine number (Chao et al., 2007; Belichenko et al., 2009; Chapleau et al., 2009; Robinson et al., 2012) as well as reduced GABA levels/GABA release (Chao et al., 2010; Gadalla et al., 2012). In contrast, studies have shown a surprising absence of altered intrinsic properties in principal cells of the *Mecp2*-null neocortex and hippocampus (Dani et al., 2005; Zhang et al., 2008). Despite this, voltage-sensitive dye measures and multiunit recording in brain slices reveal hyper-excitability of phenotypes when viewed at the hippocampal network level (Calfa et al., 2011).

The aim of the current study was to investigate seizure threshold in a mouse model of RTT and to further characterize alterations in hippocampal network excitability resulting from MeCP2 deficiency.

EXPERIMENTAL PROCEDURES

Mecp2-stop mice

Heterozygous ($Mecp2^{stop/+}$) female mice in which the endogenous *Mecp2* allele is silenced by a targeted stop cassette ($Mecp2^{tm2Bird}$, Jackson Laboratories stock No. 006849) were used as a breeding stock and backcrossed onto a C57BL6/J background by crossing with wild type (WT) C57BL6/J males (Harlan, UK). The genotype of the mice was determined by PCR (Guy et al., 2007). Unless otherwise stated, experiments were conducted using hemizygous ($Mecp2^{stop/y}$) male mice and wild-type male littermates aged 6–10 weeks. Whole-cell patch clamp studies were conducted using adult heterozygous female mice ($Mecp2^{+/stop}$) and female wild-type littermates ($Mecp2^{+/+}$) aged 35–125 days. A subset of female mice used in the study had a *Mecp2*-GFP fusion allele (Mecp2tm3.1Bird, Jackson Laboratories stock No. 014610) to aid cellular identification and these heterozygous mice were of a $Mecp2^{GFP/stop}$ genotype. Neurons from these mice advertised their MeCP2 status by the presence or absence of GFP fluorescence in living cells (Fig. 6). In a subset of seizure experiments (Fig. 1D), hemizygous null ($Mecp2^{-/y}$) and heterozygous $Mecp2^{+/-}$ (Guy et al., 2001) mice backcrossed to a C57BL6/J background, aged 6–10 weeks, and their WT littermates were used.

Mice were housed in groups with littermates, maintained on a 12-h light/dark cycle and provided with food and water *ad libitum*. Experiments were carried out in accordance with the European Communities Council Directive (86/609/EEC) and a project license with local ethical approval under the UK Animals (Scientific Procedures) Act 1986.

Kainate administration and seizure scoring *in vivo*

Animals were injected with kainic acid (25 mg/kg IP in 0.9% saline) or saline (vehicle control) and for most experiments maintained under light isoflurane anaesthesia (2.5–3% delivered to the observation chamber at a flow rate of 0.5 l/min) to reduce animal suffering. The use of anaesthesia aided accurate seizure scoring as there was not confounding locomotor activity. Mice were monitored in a $33 \times 21 \times 20$-cm high Perspex observation box. A subset of experiments was conducted in the absence of anaesthesia to exclude potential genotype-specific differences in anaesthetic sensitivity as a confounding factor. Mice were monitored and scored in real time by a trained observer. For playback and confirmation purposes, mice were additionally monitored by constant video capture using a video camera mounted below the transparent observation box. Seizure score was adapted from a previously documented scale (Racine, 1972): 0 = mice lying still with controlled breathing, 1 = lying still with fast breathing, 2 = demonstrate erratic twitches, 3 = develop a straight tail with or without a shake, 4 = forepaws begin to shake, 5 = display a straight tail together with forepaw shaking (one time), 6 = continuously (>2) show an extended tail shake with forepaw shaking, 7 = display full tonic-clonic seizures, 8 = death. At the end of the observation period, animals were killed humanely by cervical dislocation.

Hippocampal slice preparation

Mice were killed humanely by cervical dislocation and brains removed and placed into oxygenated (95% O_2, 5% CO_2) ice cold sucrose artificial cerebrospinal fluid (sACSF) containing (in mM): 87 NaCl, 25 KCl, 25 $NaHCO_3$, 1.25 NaH_2PO_4, 25 glucose, 75 sucrose, 7 $MgCl_2$, 0.5 $CaCl_2$, 1 pyruvate and 1 ascorbate. Transverse hippocampal tissue slices (400-μm and 300-μm thick for extracellular and whole-cell experiments, respectively) were cut on a vibrating microtome (Leica VT1000, Milton Keynes, UK). Slices were transferred to a submerged storage chamber containing oxygenated sACSF maintained at 34 °C. After 30 min slices were either placed directly into a recording chamber (below) or kept at 21 °C in the same chamber for later use.

Extracellular recording

Slices were transferred to an interface-type recording chamber maintained at 34 °C and perfused (flow rate = 6 ml/min) with oxygenated with ACSF containing (in mM): 124 NaCl, 3 KCl, 26 $NaHCO_3$, 1.41 NaH_2PO_4, $MgCl_2$, 9.09 glucose and 2 $CaCl_2$ where they were left to equilibrate for a further 30–60min. Recording electrodes were pulled from standard wall borosilicate (1.2 mm o.d.) tubing using a Brown and Flaming-type horizontal electrode puller (Sutter Inst., USA). Extracellular recording and stimulation electrodes were filled with ACSF and exhibited a dc resistance of 1–5 MΩ. A stimulating electrode was positioned in the Schaffer-collateral afferent pathway at the CA3/CA1 border and a recording electrode placed in the *stratum radiatum* of area CA1 to record evoked field excitatory postsynaptic potentials (fEPSPs) as well as spontaneous or

drug-induced extracellular field potential events. Recordings were amplified (10×) using an Axoclamp 2A amplifier (Molecular Devices, USA) in bridge mode, filtered (10 kHz) and further amplified (100×) using a Brownlee Model 440 Signal Processor (Brownlee Precision Co., USA). Signals were digitized at 10 kHz (Digidata 1322A, Axon Instruments) and stored on a PC hard disc using WinWCP (Anderson and Collingridge, 2001) for recording of evoked events and digitized at 1 kHz (Axon Minidigi) using Axoscope (Molecular Devices, USA) and stored on a separate PC for continuous monitoring of spontaneous events. For kainic acid experiments, recording electrodes were placed in area CA3 *stratum radiatum* and signals amplified (1000×) and low-pass filtered at 100 Hz using a Brownlee model 440 Signal processor before being digitized at 4 kHz onto PC hard disc using Axoscope (Molecular devices, USA). Signals were analysed off-line using Axograph software.

Whole-cell recording

Hippocampal slices (300-μm thickness) were transferred to a submerged style recording chamber perfused (flow rate = 6 ml/min) with oxygenated ACSF containing (in mM): NaCl (125), KCl (2.5), $NaHCO_3$ (25.0), $NaH_2PO_4{\cdot}2H_2O$ (1.25), Glucose (25.0), ascorbate (1.0), pyruvate (1.0), $MgCl_2$ (1.0) and $CaCl_2$ (2.0) where they were left to equilibrate for a further 15 min at 30–32 °C. Glass microelectrodes (2.5–3.5 MΩ resistance) were back filled with an intracellular solution consisting of (in mM): potassium gluconate (130.0), KCl (10.0), $MgCl_2$ (2.0), EGTA (10.0), HEPES (10.0), Na_2ATP (2.0), Na_2GTP (0.3), Na_2 phosphocreatine (1.0), and biocytin (0.1%). Pipettes used for stimulus electrodes were backfilled with 2 M NaCl.

Putative CA1 pyramidal cells were selected under infrared differential interference contrast (IR-DIC) video microscopy (Olympus BX50WI). Recordings were obtained using an Axoclamp 2B (Molecular Devices, USA) and data sampled at 20 KHz using a Digidata 1440 (Molecular Devices, USA) and recorded using pClamp v10.2 (Molecular Devices). Signals were filtered at 10 kHz using a Brownlee Model 440 Signal Processor (Brownlee Precision Co., Palo Alto, CA, USA). Resting membrane potential was determined shortly after establishing whole-cell configuration (< 3 min). Cells were rejected if either series resistance > 30 MΩ, resting membrane potential was less than −50 mV or action potentials were non-overshooting. Capacitance and series resistance compensation were applied. Intrinsic properties and discharge pattern were measured in current clamp mode via a series of injected hyper-depolarizing current pulses (500-ms duration, −250 pA to +250 pA, step 50 pA). Additionally, 10 pA, 500-ms current pulses were applied to measure input resistance and the membrane decay time constant (Tau).

Evoked synaptic properties were obtained in voltage clamp with cells held at −65 mV. A stimulus pipette was placed within the Schaffer-collateral/commissural pathway in the *stratum radiatum,* approximately 50 μm from stratum pyramidale and 50–100 μm from the tip of the recording neuron. Several protocols were run in order to assess short-term plasticity properties.

Data analysis

For extracellular bicuculline and 4-AP experiments event analysis was conducted offline using Stimfit analysis package (courtesy of C. Schmidt-Hieber, University College London; evoked EPSPs) and Clampfit 9.0 software (Molecular devices, USA; spontaneous field potentials). Event analysis for extracellular kainate experiments were conducted offline using Axograph X software (Axograph.com). Fast fourier transform (FFT) was used on each 2-min recording to create a power spectrum of gamma oscillations formed, by averaging segments of 1024 data points. Power was calculated as the area under each power spectrum between 20 and 80 Hz and dominant frequency was taken as the highest peak in this region. Samples were defined as epileptic and removed if moderate levels of spontaneous spiking events were detected in the baseline recording.

For the intrinsic properties the mean value of three recordings per cell was taken. Evoked paired-pulse characteristics and frequency-dependent facilitation measures were obtained from the average of 10–20 traces. Paired-pulse ratios were the ratios of the amplitude of the second pulse compared to the amplitude of the first. Similarly, the frequency facilitation pulse train was the amplitudes of the second to tenth pulse normalized to the first.

Drug administration *in vitro*

Bicuculline, NBQX (Abcam Biochemicals, UK), 4-AP (Sigma–Aldrich, UK) and kainic acid (Abcam Biochemicals, UK) were dissolved in ACSF to make 1000x stock solutions and stored as frozen aliquots prior to addition to the perfusing ACSF.

Immunohistochemistry

Following whole-cell recording, hippocampal slices were fixed (4% formaldehyde in 0.1 M phosphate buffer, PB, pH7.4) for 1–2 h at 4 °C and then transferred to 0.1 M PB and stored at 4 °C. Subsequently slices were washed three times in 0.1 M PB and again in 0.3 M phosphate-buffered saline (PBS) before blocked for one hour with 5% normal goat serum. Slices were then incubated with 1:500 polyclonal rabbit anti-MeCP2 primary antibody (Millipore, UK) in 0.3 M PBS containing 0.3% TritonX-100 for 2–3 days at 4 °C. Slices were then washed in 0.3 M PBS and incubated with Alexa Fluor 488 anti-rabbit secondary (Invitrogen, UK; 1:1000) plus avidin-conjugated Alexa Fluor 647 (Invitrogen; 1:1000) overnight at 4 °C. Wild-type and MeCP2-GFP slices were only incubated with avidin-conjugated Alexa Fluor 647 (Invitrogen, 1:1000) overnight. Finally, slices were washed in 0.3 M PBS before mounted in Vectashield (Vector Laboratories, UK) and subsequently imaged on a laser-scanning confocal microscope (Bio-Rad Radiance 2100, UK).

Statistics

The data were compared by a Student's unpaired *t*-test (maximal seizure score *in vivo*), Logrank test (seizure onset *in vivo*), non-parametric Mann–Whitney *U* test (*in vitro* kainate experiments), two-way analysis of variance (ANOVA) with Tukey's *post hoc* test (bicuculline and 4-AP data), one-way ANOVA (intrinsic single cell properties) and multivariate analysis of variance (MANOVA) (single cell paired-pulse and frequency facilitation data). All data expressed as mean ± standard error of the mean (SEM) and analysed using Prism (Graphpad.com) with statistical significance accepted at $p < 0.05$. Analysis of ictal-like events used Barnard's exact test (MATLAB, Mathworks.co.uk).

RESULTS

Mecp2$^{stop/y}$ mice have a heightened sensitivity to kainate-induced seizures *in vivo*

Epilepsy is a prominent feature in RTT syndrome patients (Hagberg et al., 2002; Neul et al., 2010) and aberrant discharge patterns have been detected in EEG recordings from *Mecp2*-null mice (D'Cruz et al., 2010). To systematically examine the propensity of mice lacking MeCP2 to develop seizures, we challenged male *Mecp2*$^{stop/y}$ mice (functional *Mecp2*-KO) and their

wild-type (WT) littermates with the convulsant drug kainic acid (25 mg/kg, IP) or with vehicle (saline). *Mecp2*$^{stop/y}$ mice were aged (6–10 weeks) at which point they were weakly symptomatic in terms of mobility, gait and breathing, etc. as described previously (Guy et al., 2007; Weng et al., 2011). Whilst none of the mice displayed overt spontaneous seizure-like activity prior to drug application, kainic acid resulted in the rapid development of seizure activity (comprising of fast breathing, erratic twitches, tail shaking, limb clonus, and tonic-clonic seizures) in both *Mecp2*$^{stop/y}$ and WT mice. However, semi-quantitative scoring of mice based on a modified Racine scale (see Experimental procedures) revealed that the proportion of mice displaying overt epileptiform signs was greater in *Mecp2*$^{stop/y}$ mice (100% of *Mecp2*$^{stop/y}$ mice develop a seizure score in contrast to 80% of WT). Moreover, the onset of seizure activity was more rapid in *Mecp2*$^{stop/y}$ mice (Fig. 1A; median onset = 10 min in *Mecp2*$^{stop/y}$ mice and 32 min in WT, $p < 0.001$, log rank test; $n = 20$ WT and 13 *Mecp2*$^{stop/y}$) and the overall seizure severity profile was greater in *Mecp2*$^{stop/y}$ mice (Fig. 1B) as was the maximal seizure score (Fig. 1C; 6 ± 0.8 in *Mecp2*$^{stop/y}$, 4 ± 0.2 in WT littermates; $p < 0.01$, unpaired *t*-test; $n = 20$ WT and 13 *Mecp2*$^{stop/y}$). In contrast to KA-injected mice, saline-injected *Mecp2*$^{stop/y}$ ($n = 8$) and WT mice ($n = 11$) displayed no seizure-like phenotypes during the 3-h recording sessions (data not shown). In order to reduce animal suffering, the above experiments were conducted under light isoflurane anaesthesia. However, there was a similar increased seizure score in *Mecp2*-KO mice versus WT when challenged with kainic acid in the absence of anaesthesia (Fig. 1D). This was also found in female *Mecp2*$^{+/-}$ mice (Fig. 1D), an accurate genetic model of RTT in girls, whereby approximately half of neurons are deficient in MeCP2 as a consequence of random X-chromosome inactivation.

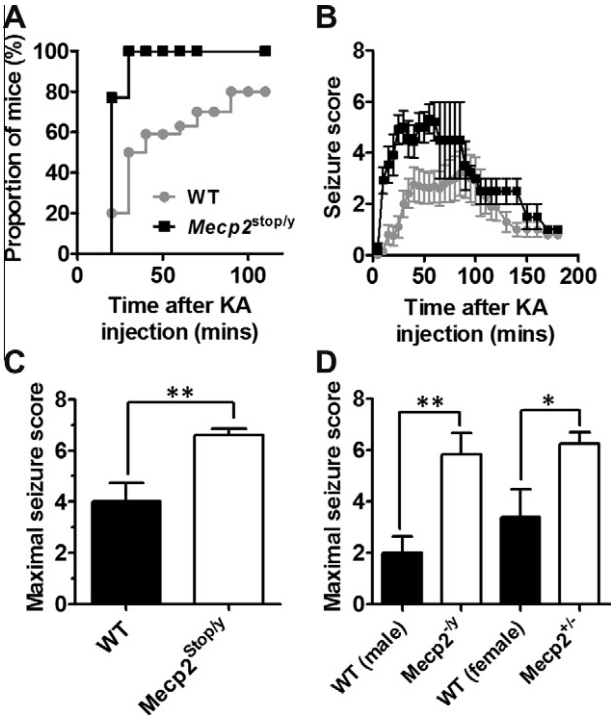

Fig. 1. Heightened sensitivity to kainate-induced seizures in *Mecp2*-$^{stop/y}$ mice. (A) Plot showing the proportion of wild-type (WT, grey circles) and *Mecp2*$^{stop/y}$ mice (black squares) displaying overt seizures following administration of kainic acid (KA, 25 mg/kg, IP). *Mecp2*$^{stop/y}$ mice show a quicker onset of seizures ($p < 0.001$, Log-rank test, $n = 20$ WT and 13 *Mecp2*$^{stop/y}$). (B) Time plot showing mean seizure score over 3 h post-KA application (same symbols as in A). (C) Column plot showing maximal seizure score in WT and *Mecp2*$^{stop/y}$ mice (n = same as above; $p < 0.01$, unpaired *t*-test). (D) Column plot comparing the maximal seizure score in wild-type (WT; *Mecp2*$^{+/y}$) and *Mecp2*$^{-/y}$ male mice and in WT (*Mecp2*$^{+/+}$) and heterozygous *Mecp2*$^{+/-}$ female mice in absence of anaesthesia (see Experimental procedures). An increase in seizure severity is observed in *Mecp2*$^{-/y}$ mice ($p < 0.01$, unpaired *t*-test, $n = 6$ mice for each genotype) and *Mecp2*$^{+/-}$ mice ($p < 0.05$, unpaired *t*-test, n = 5–8 mice for each genotype) when compared against their WT controls. All data expressed as mean ± SEM.

Altered gamma network oscillations in the hippocampus of *Mecp2*$^{stop/y}$ mice

To further investigate oscillatory network activities *in vitro* and to assess the network level epileptiform phenotype potentially underlying the heightened sensitivity to kainate-induced seizures (Fig. 1), we applied kainic acid to hippocampal slices prepared acutely from *Mecp2*$^{stop/y}$ mice and their WT littermates. Under control conditions (prior to kainic acid), slices from both WT and *Mecp2*$^{stop/y}$ mice did not show detectable spontaneous oscillatory field potential activity (Fig. 2). However, application of 400 nM kainic acid resulted in the gradual appearance of regular gamma frequency network oscillations (mean peak frequency = 33 ± 1.7 Hz, $n = 26$ slices from nine mice). The kainate-induced oscillations were similar to previous descriptions (Hajos et al., 2000; Fisahn et al., 2004) and were abolished upon co-application of the glutamate-receptor blocker NBQX (5 μM; $n = 26$ slices from nine mice; Fig. 2Ai–iii). The magnitude of the kainic acid-induced oscillatory activity was typically greater in the *Mecp2*$^{stop/y}$ slices (Fig. 2A, B) and examination of oscillatory activity by power spectrum analysis revealed that slices from *Mecp2*$^{stop/y}$ mice display a more prominent gamma frequency peak compared to wild-type slices (Fig. 2Aiv, Biv and C). Analysis of pooled data revealed a significant difference in mean power (see Experimental procedures) between genotypes (Fig. 2D; 252 ± 118 μV^2 for WT compared to 1059 ± 379 μV^2 in *Mecp2*$^{stop/y}$ slices, $p < 0.01$, Mann–Whitney *U* test, n = 26–14 slices, respectively). In contrast, there was no significant difference in dominant frequency between slices of each genotype (Fig. 2E; WT = 33 ± 1.7 Hz, $n = 26$ slices; *Mecp2*$^{stop/y}$ = 35 ± 2.1 Hz, $n = 14$ slices; $p = 0.579$, Mann–Whitney *U* test).

Altered properties of bicuculline-induced epileptiform activity in the hippocampus of *Mecp2*$^{stop/y}$ mice

To further assess differences in network excitability in the MeCP2-deficient brain we investigated epileptiform network activities resulting from compromised GABAergic inhibition. Hippocampal slices from

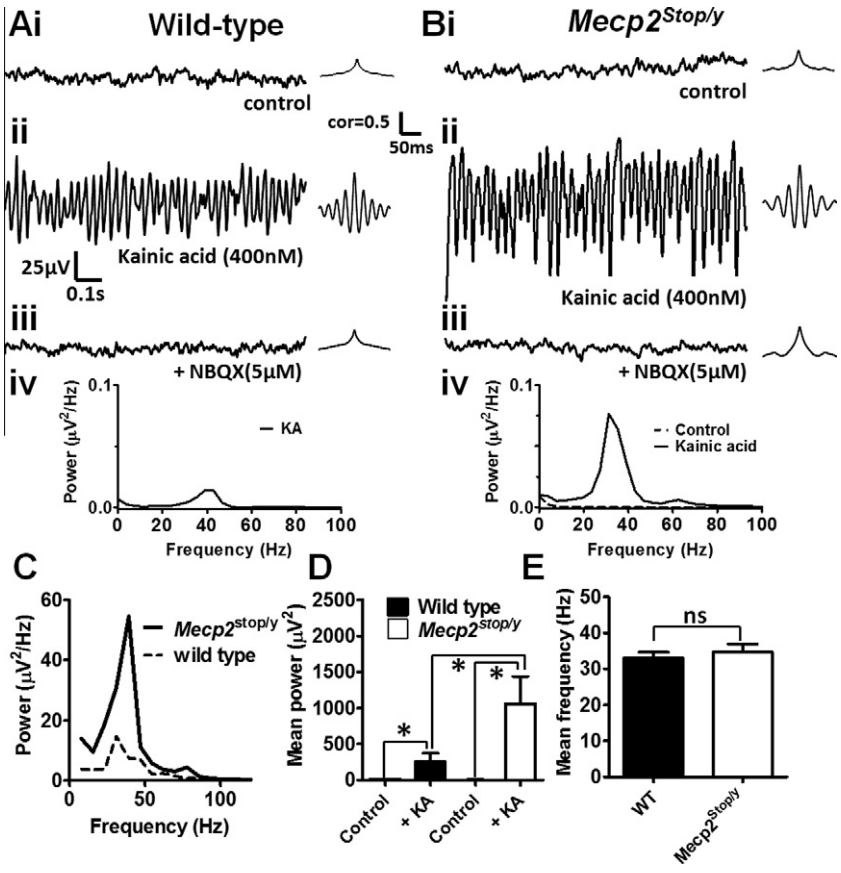

Fig. 2. Increased power of gamma frequency network oscillations in hippocampal slices from *Mecp2*$^{stop/y}$ mice. (A) Representative extracellular field potential traces from WT hippocampus showing (i) baseline quiescence prior to application of kainic acid (400 nM) following which (ii) trace becomes dominated by a gamma frequency (~30–40 Hz) oscillation. This network oscillation was abolished following administration of the AMPA-receptor antagonist NBQX (5 μM). (iv) Power spectrum from same experiments showing oscillation with a dominant frequency at ~40 Hz. Inserts at end of each trace are corresponding autocorrelation plots which reveal the presence of regular oscillation in KA-treated slices. (B) Similar representative data plots from a *Mecp2*$^{stop/y}$ mouse hippocampal slice. Note the more prominent and higher power gamma frequency oscillation relative to the WT traces. (C) Pooled data showing average power spectra from WT (n = 26 slices from nine mice) and *Mecp2*$^{stop/y}$ samples (n = 14 slices from six mice). (D) Column plot showing mean gamma oscillation power before and following KA application in WT and *Mecp2*$^{stop/y}$ samples revealing a significant difference in mean power between genotypes (p > 0.01, Mann–Whitney U test, n = 14–26 slices per genotype). (E) Plot showing dominant frequency which did not differ between genotypes (p = 0.58, Mann–Whitney U test, n = 14–26 slices per genotype). Scale bars = voltage traces, 25 μV, 0.1 s; correlation = 0.5, 50 ms.

Mecp2$^{stop/y}$ mice and their wild-type littermates were perfused with increasing concentrations of the $GABA_A$-receptor antagonist bicuculline and extracellular field recordings obtained from the stratum radiatum in area CA1. In addition to monitoring spontaneous baseline events, evoked synaptic potentials were monitored by electrical stimulation of efferent fibres in the stratum radiatum at the CA3/CA1 border. Bath application of bicuculline (0.1–10 μM) resulted in a concentration-dependent increase in the occurrence of spontaneous epileptiform bursting events (Fig. 3A, B) as described previously (Roshan-Milani et al., 2003). Over the lower concentration range (0.1, 1 and 3 μM bicuculline), slices from *Mecp2*$^{stop/y}$ mice showed a greater frequency of spontaneous bursting compared to WT (Fig. 3B; p < 0.05, two-way ANOVA with Tukey's *post hoc* test; n = 18 slices, from five wild-type mice and n = 22 slices from five *Mecp2*$^{stop/y}$ mice). At the highest concentration tested (10 μM bicuculline), there was no difference between genotypes in terms of burst frequency. However, further analysis of spontaneous epileptiform events (Fig. 3C) revealed the duration of spontaneous epileptiform bursts to be longer in slices from *Mecp2*$^{stop/y}$ mice (626 ± 55 ms) compared to WT littermate controls (366 ± 34 ms) after application of 10 μM bicuculline (Fig. 3C; p < 0.001, two-way ANOVA with Tukey's *post hoc* test). Similarly, analysis of the duration of synaptic stimulation-evoked epileptiform bursts showed a greater duration of epileptiform burst event in *Mecp2*$^{stop/y}$ slices (Fig. 3D; 416 ± 66 ms compared to 83 ± 25 ms in wild-type slices; p < 0.05, two-way ANOVA with Tukey's *post hoc* test).

Altered properties of 4-aminopyridine-induced epileptiform activity in the hippocampus of *Mecp2*$^{stop/y}$ mice

In contrast to bicuculline-induced disinhibition of networks, the potassium channel blocker 4-aminopyridine promotes epileptiform activity via neuronal depolarization and

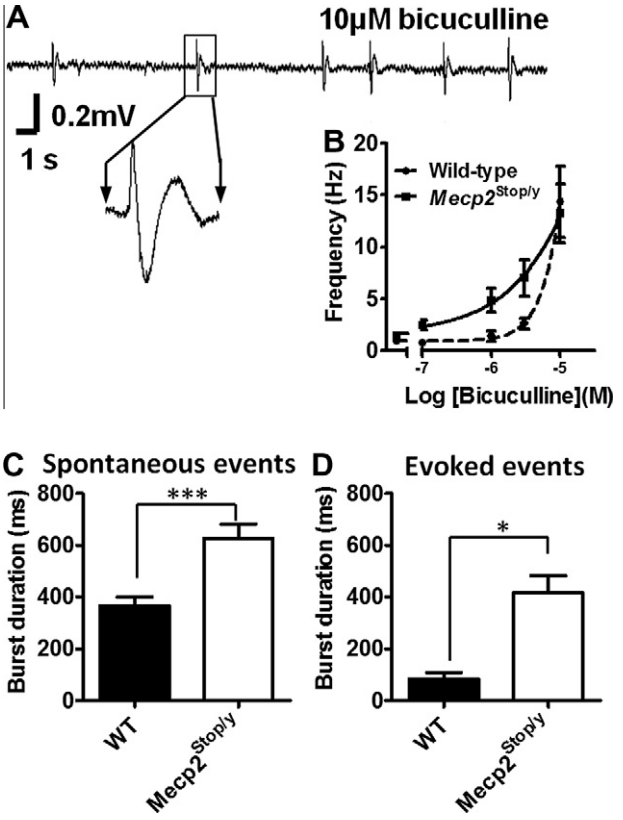

Fig. 3. Altered properties of bicuculline-induced epileptiform activity in hippocampal slices from *Mecp2*$^{stop/y}$ mice. (A) Representative extracellular field potential recording in area CA1 showing characteristic spontaneous epileptiform bursting activity in response to application of the $GABA_A$-receptor antagonist bicuculline (10 μM). Insert shows individual burst event. (B) Plot showing frequency of epileptiform bursting in response to increasing bath concentrations of bicuculline (0.1–10 μM). There was a significant difference in burst frequency between genotypes at 0.1–1 μM concentrations ($p < 0.05$, two-way ANOVA with Tukey's *post hoc* test, $n = 18$ slices, from five WT mice and $n = 22$ slices from five *Mecp2*$^{stop/y}$ mice). (C, D) Plots showing increased duration of spontaneous ($p < 0.001$, two-way ANOVA with Tukey's *post hoc* test) and electrical stimulation-evoked epileptiform bursts ($p < 0.05$, two-way ANOVA with Tukey's *post hoc* test) in slices from *Mecp2*$^{stop/y}$ mice in the presence of 10 μM bicuculline (same *n* as above). Scale bar = 0.2 mV, 1 s.

strengthened glutamatergic signalling (Traub and Jefferys, 1994). To further evaluate hippocampal network excitability, we applied the 4-AP to hippocampal slices from *Mecp2*$^{stop/y}$ mice and their wild-type littermates and monitored spontaneous and evoked epileptiform events as above. Increasing concentration of 4-AP resulted in the appearance and then increasing incidence of epileptiform events in slices from both genotypes (Fig. 4A–C). No difference was observed in the frequency of epileptiform bursts between genotypes over the low concentration range (1, 3, 10, and 30 μM, all $p > 0.05$ way ANOVA with Tukey's *post hoc* test, $n = 12$ slices per genotype). However, at the highest concentration tested, there was a significantly higher frequency of spontaneous epileptiform events in slices from *Mecp2*$^{stop/y}$ mice compared to littermate WT controls (Fig. 4C; 50 μM, $p < 0.05$, two-way ANOVA with Tukey's *post hoc* test, $n = 12$ slices per genotype). An analysis of burst duration revealed both the duration of the spontaneous (134 ± 24 ms for WT; 203 ± 24 ms for *Mecp2*$^{stop/y}$ mice) epileptiform burst events and electrical (15 ± 3 ms for WT; 93 ± 12 ms for *Mecp2*$^{stop/y}$ mice) stimulation-evoked epileptiform bursts was longer in slices from *Mecp2*$^{stop/y}$ mice ($p < 0.05$, two-way ANOVA with Tukey's *post hoc* test) compared to WT controls upon application of 50 μM 4-AP (Fig. 4D, E).

In addition to an increase in the frequency and duration of epileptiform burst-like events (Fig. 4), 50 μM 4-AP also resulted in the appearance of more complex 'ictal-like' field potential events (Fig. 5) characterized by a high-frequency discharge followed by a train of

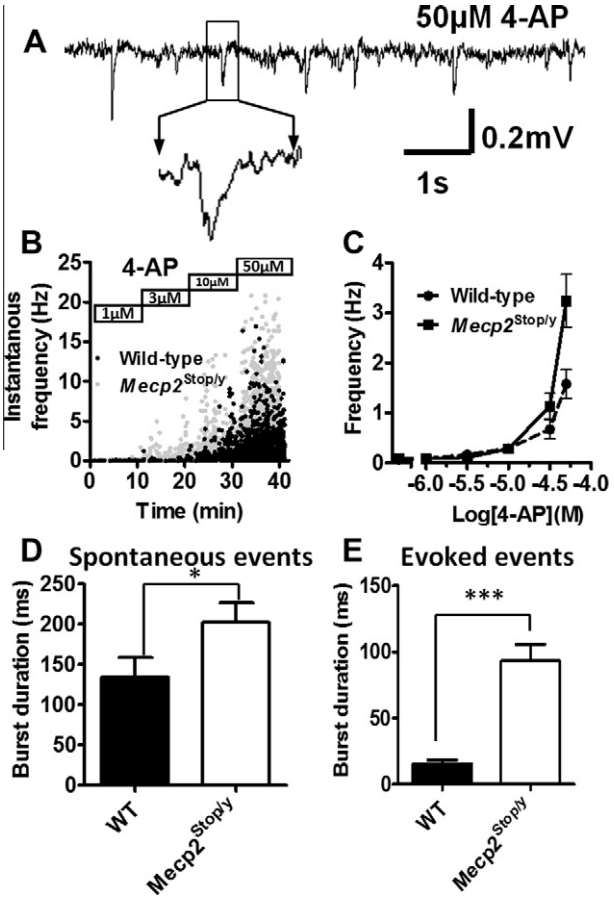

Fig. 4. Altered properties of 4-aminopyridine-induced epileptiform activity in hippocampal slices from *Mecp2*$^{stop/y}$ mice. (A) Representative extracellular field potential recording in area CA1 showing characteristic spontaneous epileptiform bursting activity in response to application of the potassium channel blocker 4-aminopyridine (4-AP, 50 μM). Insert shows individual burst event. (B) Scatter plot showing instantaneous burst frequency in representative recordings from WT (black symbols) and *Mecp2*$^{stop/y}$ (grey symbols) slices in response to increasing bath concentration of 4-AP. (C) Plot showing pooled epileptiform burst frequency data in response to increasing bath concentrations of 4-AP (1–50 μM). There was a significant difference in burst frequency between genotypes at the highest concentration tested (50 μM, $p < 0.05$, two-way ANOVA with Tukey's *post hoc* test, $n = 12$ slices per genotype). (D,E) Plots showing increased duration of spontaneous ($p < 0.05$, two-way ANOVA with Tukey's *post hoc* test) and electrical stimulation-evoked epileptiform bursts ($p < 0.05$, two-way ANOVA with Tukey's *post hoc* test) in slices from *Mecp2*$^{stop/y}$ mice in the presence of 50 μM 4-AP (same *n* as above). Scale bar = 0.2 mV, 1s.

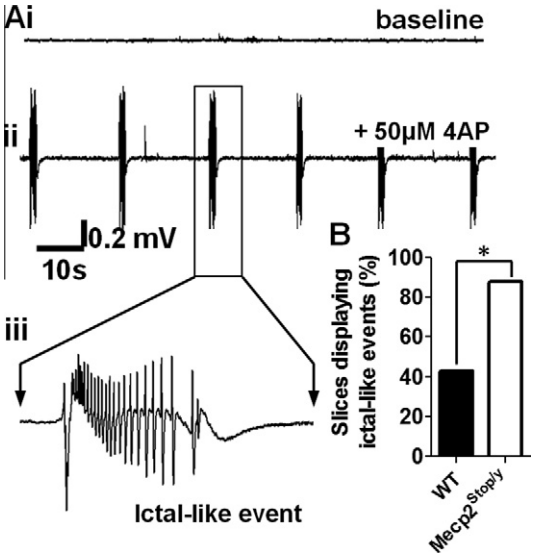

Fig. 5. Hippocampal networks from *Mecp2*$^{stop/y}$ mice have a greater propensity to display ictal-like events in response to 4-aminopyridine challenge. (Ai) Representative field potential recording from a *Mecp2*$^{stop/y}$ hippocampus displaying typical baseline quiescence. (ii) Subsequent application of 4-AP (50 μM) results in the appearance of characteristic ictal-like events (high-frequency discharge followed by train of burst-like events) as shown in insert (iii). (B) Column plots showing that the occurrence of ictal-like is more commonly observed in slices from *Mecp2*$^{stop/y}$ mice compared to WT ($p < 0.05$, Barnard's test, $n = 3$ from a total of 7 slices for WT and $n = 8$ from a total of 9 slices for *Mecp2*$^{stop/y}$ mice). Scale bar = 0.2 mV, 10 s).

burst-like events (Fig. 5Aiii). These complex prolonged network discharges were more common in slices from *Mecp2*$^{stop/y}$ mice (88%) compared to slices from WT mice (43%) (Fig. 5B; $p < 0.05$, Barnard's test; $n = 7$ and 9 for WT and *Mecp2*$^{stop/y}$ mice, respectively).

Cellular level excitability in MeCP2-deficient hippocampal neurons

To investigate potential factors that may contribute towards network hyper-excitability and enhanced propensity for epileptiform activities we went onto assess intrinsic excitability at the level of single neurons. Hippocampal slices prepared from female heterozygous (*Mecp2*$^{+/stop}$) mice enabled the direct characterization of neurons expressing MeCP2 protein or devoid of MeCP2 (Fig. 6A, B). We first examined passive and active intrinsic properties by performing whole-cell patch clamp recordings from CA1 pyramidal cells. Overall there was no significant difference in resting membrane potential, input resistance, membrane time constant or any other passive properties measured between cells expressing MeCP2 (MeCP2+ve) and cells devoid of MeCP2 (MeCP2–ve) either from heterozygous brains or from WT mice (Table 1; all $p > 0.05$, ANOVA; $n = 10$–14 cells per group). Similarly, there were no differences across a range of active properties such as action potential amplitude, kinetics (Table 1 and Fig. 6) and action potential frequency in response to increasing current injection (Fig. 6D; $p = 0.648$, MANOVA).

To examine potential differences in evoked excitatory transmission, EPSCs were monitored in CA1 pyramidal cells upon stimulation of Schaffer-collateral afferents in the *stratum radiatum*. The waveform and kinetics were similar for all (WT and MeCP2+ve and MeCP2-ve in *Mecp2*$^{stop/y}$) cell types (Fig. 6E, EPSC 20–80% rise time: WT = 1.55 ± 0.12 ms, MeCP2−ve = 1.69 ± 0.15 ms, MeCP2+ve = 1.49 ± 0.12 ms, $p = 0.584$, ANOVA; decay time constant: WT = 8.93 ± 1.3 ms, MeCP2−ve = 8.94 ± 1.08 ms, MeCP2+ve = 9.72 ± 1.31 ms, $p = 0.39$, ANOVA; $n = 9$–12 cells per group) and all three showed similar levels of paired-pulse facilitation when tested at a range of inter-stimulus intervals (Fig. 6F; $p = 0.576$, MANOVA, $n = 10$–13 per group). Finally, evoked postsynaptic frequency facilitation in response to longer trains (10 pulse) 40-Hz afferent stimulation (Fig. 6G) revealed no differences in normalized amplitudes between genotypes (Fig. 6H; $p = 0.382$, MANOVA, $n = 9$–13 cells per group). Similar results were obtained for 5-, 10- and 20-Hz pulse trains (data not shown).

DISCUSSION

Epilepsy is a prominent feature of RTT patients (Hagberg et al., 2002; Glaze, 2005; Glaze et al., 2010) yet *Mecp2*$^{-/y}$ mice are reported to very rarely develop full electrographic seizures (Chao et al., 2010). The main finding of the current report was the demonstration that silencing/deletion of *Mecp2* in mice resulted in a heightened susceptibility to seizures when challenged with a convulsant drug paradigm (kainic acid). Whilst not showing any overt seizure phenotype under homecage conditions, these mice nevertheless demonstrated an underlying sensitivity when challenged with kainic acid, developing a more severe and rapid onset seizure phenotype. This enhanced sensitivity to display seizures was apparent in both hemizygous male mice, in which the entire brain (and periphery) is deficient of MeCP2, as well as in heterozygous female mice displaying a mosaic expression of MeCP2-containing and MeCP2-deficient cells. This result suggests that the absence of functional MeCP2 in a subset of cells is sufficient to result in a predisposition to seizures. These findings point to MeCP2-deficiency bringing the brain closer to seizure threshold and suggest that there may be underlying altered brain network excitability. This would be consistent with previous reports of abnormal EEG patterns in the *Mecp2*-null mouse (D'Cruz et al., 2010) and cellular level studies showing alterations in excitation/inhibition balance (Dani et al., 2005) and spread of excitatory discharge (Calfa et al., 2011). Abnormal EEG and seizures have also been reported in *Mecp2*$^{308/y}$ mice expressing a truncated form of MeCP2 (Shahbazian et al., 2002). The levels of functional MeCP2 may therefore have a profound influence on network excitability and seizure generation and indeed overexpression/duplication of *MECP2* is also reported to produce epilepsy phenotypes in both patients (Ramocki et al., 2009) and in mice (Collins et al., 2004).

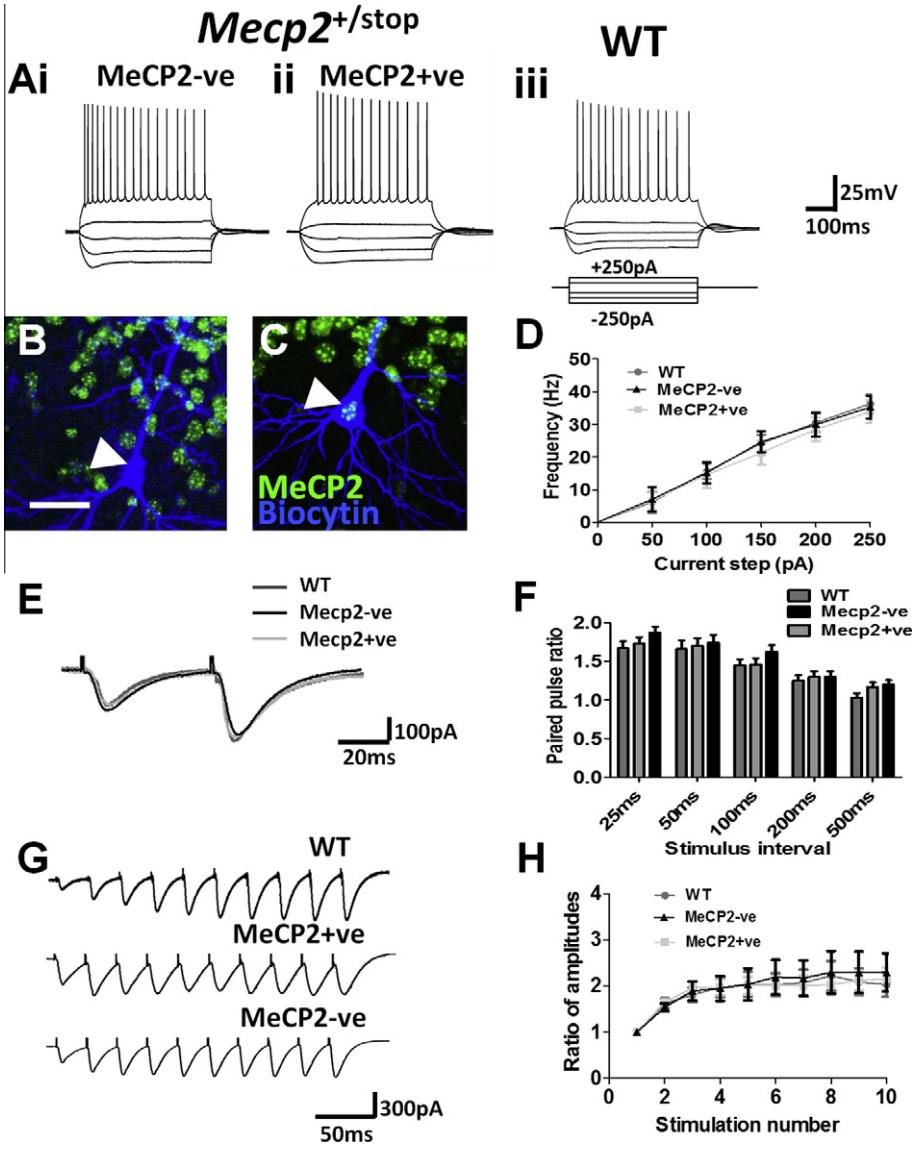

Fig. 6. Cellular-level excitability is unaltered in MeCP2-deficient neurons. (A) Representative current clamp traces in response to hyperpolarizing and depolarizing pulses (500 ms; −250 pA to +250 pA, 50 pA steps) in heterozygous MeCP2+ve and MeCP2−ve (i–ii) and WT CA1 pyramidal cells (iii). (B, C) Representative confocal images of biocytin filled MeCP2+ve (right) and MeCP2−ve (left) cells. Note the absence of MeCP2 nuclear immunoreactivity in the MeCP2-deficient cell. (D) Plot of mean action potential frequency versus current injection for each cell type (p = 0.648, MANOVA, n = 10–14 cells per group; n = 8–13 mice for each genotype). (E) Example of evoked EPSCs from all three cell types (overlaid) in response to paired stimulation of Schaffer-collateral afferents. Note the similar kinetics between genotypes and cells of different MeCP2 status. (F) Comparison of paired-pulse facilitation ratios across 25–500 ms stimulus intervals. There was no significant difference between the three cell types (p = 0.576, MANOVA). (G) Representative examples of frequency facilitation in response to 40-Hz afferent stimulation. (H) Pooled frequency facilitation amplitude data (normalized to the first pulse) showing no significant difference between cell types (p = 0.382, MANOVA test). Scale bars = current clamp traces = 25 mV, 100 ms; confocal images = 25 μM; frequency facilitation traced = 300 pA, 50 ms; paired-pulse traces = 100 pA, 20 ms).

The seizure phenotype observed at the whole animal level was mirrored at the neuronal network (hippocampal) level by a heightened epileptiform response to convulsant drugs acting via discrete mechanisms. Epileptiform bursts produced through either disinhibition ($GABA_A$-receptor blockade) or direct excitation (K^+ channel blockade) were more pronounced in slices from $Mecp2^{stop/y}$ mice, both in terms of enhanced frequency and prolonged burst duration. The genotype-related difference in epileptiform activity was not apparent at the highest concentration of bicuculline tested. This might suggest compromised GABAergic inhibition may be an important factor in the MeCP2-deficient brain but that levels of network excitability are equivalent when inhibition is completely abolished by very high $GABA_A$-receptor antagonist concentrations. This would be consistent with reduced levels of GABA release reported in *Mecp2*-knockout brains (Chao et al., 2010; Gadalla et al., 2012).

In contrast to the bicuculline and 4-aminopyridine experiments, the addition of kainic acid to hippocampal slices resulted in a gamma frequency network oscillation that is considered to be more consistent with

Table 1. Biophysical properties of pyramidal cells in hippocampal area CA1 of wild-type and *Mecp2*$^{+/stop}$ mice. No significant differences were observed between MeCP2-containing (MeCP2 + ve) and MeCP2-deficient (MeCP2 − ve) pyramidal cells in the mosaic *Mecp2*$^{+/stop}$ mouse brain (% difference shown in right column) and between pyramidal cells in wild-type mice (all $p > 0.05$, ANOVA, $n = 10–14$ for each cell type)

Intrinsic property	Wild type (MeCP2 + v)	*Mecp2*$^{+/stop}$		
		MeCP2 + ve	MeCP2 − ve	% Change
Resting membrane potential (mV)	−61.7 ± 1.6	−60.2 ± 1.4	−62.2 ± 1.92	−2%
Membrane time constant (ms)	31.4 ± 2.6	26.7 ± 1.9	25.2 ± 3.2	+6%
Input resistance (MΩ)	125.8 ± 11.0	143.8 ± 15.1	159.1 ± 13.7	+11%
Threshold (mV)	−37.7 ± 0.7	−37.7 ± 1.8	−39.4 ± 1.7	+5%
Amplitude (mV)	84.2 ± 2.8	83.6 ± 1.8	86.4 ± 2.0	+3%
20–80% rise time (ms)	0.08 ± 0.01	0.08 ± 0.004	0.09 ± 0.01	+12%
½ Height duration (ms)	1.04 ± 0.06	1.05 ± 0.02	1.15 ± 0.06	+10%
Maximal rise rate (mV ms^{-1})	582 ± 41	583 ± 27	546 ± 41	−6%
Maximal decay rate (mV ms^{-1})	106 ± 7	101 ± 3	94 ± 5	−7%
Medium AHP amplitude (mV)	11.1 ± 4.3	9.4 ± 0.8	10.2 ± 0.9	−8%

behaviour-related physiological network processes (Traub et al., 1998; Whittington et al., 2011). However, there was a clear difference between genotypes with slices from *Mecp2*$^{stop/y}$ mice showing higher power gamma frequency network oscillations. This is consistent with MeCP2-deficient hippocampal networks predisposed to hyperexcitability and hypersynchrony. Indeed, the kainic acid-induced gamma oscillations in the *Mecp2*$^{stop/y}$ hippocampal slices were often observed to display a jagged waveform consistent with a more epileptiform signal. This may represent an altered behaviour in the MeCP2-deficient hippocampus in which there is a transition in activity from physiological oscillatory rhythms to a more pathological state. This was observed also in the 4-aminopyridine experiments where slices from *Mecp2*$^{stop/y}$ mice were more likely to switch from bursting activity to full ictal-like discharge patterns. The fact that dominant gamma band frequency was similar between genotypes suggests that circuits generating gamma oscillatory activity are not tuned to a different frequency *per se* but rather the ensemble activity is more pronounced in the *Mecp2*$^{stop/y}$ hippocampal slices. This parallels recent findings in a T158A model of RTT (knock-in of a common human mutation) in which the authors observed an increase in the high gamma frequency power EEG activity (Goffin et al., 2012), conspicuous before and during seizures (Uhlhaas et al., 2011), and consistent with a hyperactivity phenotype in *Mecp2*-null mice (Chao et al., 2010).

The overt differences in network level behaviour observed between genotypes at the whole animal and hippocampal network levels were not apparent at the single-cell level. Indeed, a comparison of MeCP2-containing and MeCP2-deficient pyramidal cells in the MeCP2-mosaic heterozygous female brain did not reveal any differences across a wide range of intrinsic properties examined in principal cells in area CA1. Whilst this result is surprising given the robust difference in network-level excitability shown in this study, it is nevertheless consistent with similar reports comparing neurons in *Mecp2*$^{-/y}$ and wild-type mouse cortex (Dani et al., 2005) and the hippocampus (Zhang et al., 2008) and following *Mecp2*-knock down (Wood et al., 2009). In addition to intrinsic biophysical properties, we did not observe differences in the properties of evoked synaptic current between cells with different MeCP2 status including short-term plasticity in response to gamma frequency afferent stimulation. However, a confounding factor when interpreting these experiments is that the afferent fibres stimulated in the heterozygous mouse brain slices will be of mixed MeCP2 status, irrespective of the known status of the postsynaptic recorded neuron. Thus, any subtle differences in presynaptic function due to MeCP2 deficiency may be masked. Whilst other groups have reported differences in evoked and spontaneous/miniature synaptic potentials (Dani et al., 2005; Nelson et al., 2006; Chao et al., 2007), the discrepancy between a network level phenotype and cellular/synaptic phenotype in this study may be due to the hyperexcitability phenotype being driven by another hippocampal area (Zhang et al., 2008; Calfa et al., 2011) or the important contribution of GABAergic circuits in the RTT phenotype (Medrihan et al., 2008; Zhang et al., 2008, 2010; Chao et al., 2010).

CONCLUSION

In conclusion, we show that MeCP2-deficient mice show an underlying pro-seizure phenotype that can be revealed by pharmacological convulsant challenge. As such, application of this seizure challenge models may be beneficial in future studies testing novel pharmacological and genetic approach therapies in RTT (Cobb et al., 2010; Gadalla et al., 2011) to establish whether putative benefits extend into the epilepsy domain of the RTT-like phenotype.

Acknowledgements—We are grateful to the MRC (Grant G0800401) and the Rett Syndrome Association Scotland for generous support. F.M. was supported by a SULSA studentship.

REFERENCES

Amir RE, Van den Veyver IB, Wan M, Tran CQ, Francke U, Zoghbi HY (1999) Rett syndrome is caused by mutations in X-linked MECP2, encoding methyl-CpG-binding protein 2. Nat Genet 23:185–188.

Anderson WW, Collingridge GL (2001) The LTP Program: a data acquisition program for on-line analysis of long-term potentiation and other synaptic events. J Neurosci Methods 108:71–83.

Asaka Y, Jugloff DG, Zhang L, Eubanks JH, Fitzsimonds RM (2006) Hippocampal synaptic plasticity is impaired in the Mecp2-null mouse model of Rett syndrome. Neurobiol Dis 21:217–227.

Belichenko PV, Wright EE, Belichenko NP, Masliah E, Li HH, Mobley WC, Francke U (2009) Widespread changes in dendritic and axonal morphology in Mecp2-mutant mouse models of Rett syndrome: evidence for disruption of neuronal networks. J Comp Neurol 514:240–258.

Calfa G, Hablitz JJ, Pozzo-Miller L (2011) Network hyperexcitability in hippocampal slices from Mecp2 mutant mice revealed by voltage-sensitive dye imaging. J Neurophysiol 105:1768–1784.

Cardoza B, Clarke A, Wilcox J, Gibbon F, Smith PE, Archer H, Hryniewiecka-Jaworska A, Kerr M (2011) Epilepsy in Rett syndrome: association between phenotype and genotype, and implications for practice. Seizure 20:646–649.

Chahrour M, Zoghbi HY (2007) The story of Rett syndrome: from clinic to neurobiology. Neuron 56:422–437.

Chao HT, Chen H, Samaco RC, Xue M, Chahrour M, Yoo J, Neul JL, Gong S, Lu HC, Heintz N, Ekker M, Rubenstein JL, Noebels JL, Rosenmund C, Zoghbi HY (2010) Dysfunction in GABA signalling mediates autism-like stereotypies and Rett syndrome phenotypes. Nature 468:263–269.

Chao HT, Zoghbi HY, Rosenmund C (2007) MeCP2 controls excitatory synaptic strength by regulating glutamatergic synapse number. Neuron 56:58–65.

Chapleau CA, Calfa GD, Lane MC, Albertson AJ, Larimore JL, Kudo S, Armstrong DL, Percy AK, Pozzo-Miller L (2009) Dendritic spine pathologies in hippocampal pyramidal neurons from Rett syndrome brain and after expression of Rett-associated MECP2 mutations. Neurobiol Dis 35:219–233.

Chen RZ, Akbarian S, Tudor M, Jaenisch R (2001) Deficiency of methyl-CpG binding protein-2 in CNS neurons results in a Rett-like phenotype in mice. Nat Genet 27:327–331.

Cobb S, Guy J, Bird A (2010) Reversibility of functional deficits in experimental models of Rett syndrome. Biochem Soc Trans 38:498–506.

Collins AL, Levenson JM, Vilaythong AP, Richman R, Armstrong DL, Noebels JL, David Sweatt J, Zoghbi HY (2004) Mild overexpression of MeCP2 causes a progressive neurological disorder in mice. Hum Mol Genet 13:2679–2689.

D'Cruz JA, Wu C, Zahid T, El-Hayek Y, Zhang L, Eubanks JH (2010) Alterations of cortical and hippocampal EEG activity in MeCP2-deficient mice. Neurobiol Dis 38:8–16.

Dani VS, Chang Q, Maffei A, Turrigiano GG, Jaenisch R, Nelson SB (2005) Reduced cortical activity due to a shift in the balance between excitation and inhibition in a mouse model of Rett syndrome. Proc Natl Acad Sci U S A 102:12560–12565.

Fisahn A, Contractor A, Traub RD, Buhl EH, Heinemann SF, McBain CJ (2004) Distinct roles for the kainate receptor subunits GluR5 and GluR6 in kainate-induced hippocampal gamma oscillations. J Neurosci 24:9658–9668.

Gadalla KK, Bailey ME, Cobb SR (2011) MeCP2 and Rett syndrome: reversibility and potential avenues for therapy. Biochem J 439:1–14.

Gadalla KKE, Bailey MES, Spike RC, Ross P, Woodard KT, Kalburgi SN, Bachaboina L, Deng JV, West AE, Samulski RJ, Gray SJ, Cobb SR (2012) Improved survival and reduced phenotypic severity following AAV9/MECP2 gene transfer to neonatal and juvenile male *Mecp2* knockout mice. Mol Ther, in press. http://dx.doi.org/10.1038/mt.2012.200. [Epub ahead of print].

Glaze DG (2005) Neurophysiology of Rett syndrome. J Child Neurol 20:740–746.

Glaze DG, Percy AK, Skinner S, Motil KJ, Neul JL, Barrish JO, Lane JB, Geerts SP, Annese F, Graham J, McNair L, Lee HS (2010) Epilepsy and the natural history of Rett syndrome. Neurology 74:909–912.

Goffin D, Allen M, Zhang L, Amorim M, Wang IT, Reyes AR, Mercado-Berton A, Ong C, Cohen S, Hu L, Blendy JA, Carlson GC, Siegel SJ, Greenberg ME, Zhou Z (2012) Rett syndrome mutation MeCP2 T158A disrupts DNA binding, protein stability and ERP responses. Nat Neurosci 15:274–283.

Guy J, Cheval H, Selfridge J, Bird A (2011) The role of MeCP2 in the brain. Annu Rev Cell Dev Biol 27:631–652.

Guy J, Gan J, Selfridge J, Cobb S, Bird A (2007) Reversal of neurological defects in a mouse model of Rett syndrome. Science 315:1143–1147.

Guy J, Hendrich B, Holmes M, Martin JE, Bird A (2001) A mouse Mecp2-null mutation causes neurological symptoms that mimic Rett syndrome. Nat Genet 27:322–326.

Hagberg B, Hanefeld F, Percy A, Skjeldal O (2002) An update on clinically applicable diagnostic criteria in Rett syndrome. Comments to Rett syndrome clinical criteria consensus panel satellite to European paediatric neurology society meeting, Baden Baden, Germany, 11 September 2001. Eur J Paediatr Neurol 6:293–297.

Hajos N, Katona I, Naiem SS, MacKie K, Ledent C, Mody I, Freund TF (2000) Cannabinoids inhibit hippocampal GABAergic transmission and network oscillations. Eur J Neurosci 12:3239–3249.

Kim HJ, Kim SH, Kim HD, Lee JS, Lee YM, Koo KY, Kang HC (2012) Genetic and epileptic features in Rett syndrome. Yonsei Med J 53:495–500.

Medrihan L, Tantalaki E, Aramuni G, Sargsyan V, Dudanova I, Missler M, Zhang W (2008) Early defects of GABAergic synapses in the brain stem of a MeCP2 mouse model of Rett syndrome. J Neurophysiol 99:112–121.

Nelson ED, Kavalali ET, Monteggia LM (2006) MeCP2-dependent transcriptional repression regulates excitatory neurotransmission. Curr Biol 16:710–716.

Neul JL, Kaufmann WE, Glaze DG, Christodoulou J, Clarke AJ, Bahi-Buisson N, Leonard H, Bailey ME, Schanen NC, Zappella M, Renieri A, Huppke P, Percy AK (2010) Rett syndrome: revised diagnostic criteria and nomenclature. Ann Neurol 68:944–950.

Ramocki MB, Peters SU, Tavyev YJ, Zhang F, Carvalho CM, Schaaf CP, Richman R, Fang P, Glaze DG, Lupski JR, Zoghbi HY (2009) Autism and other neuropsychiatric symptoms are prevalent in individuals with MeCP2 duplication syndrome. Ann Neurol 66:771–782.

Robinson L, Guy J, McKay L, Brockett E, Spike R, Selfridge J, De Sousa D, Merusi C, Riedel G, Bird A, Cobb SR (2012) Morphological and functional reversal of phenotypes in a mouse model of Rett syndrome. Brain 135:2699–2710.

Roshan-Milani S, Ferrigan L, Khoshnood MJ, Davies CH, Cobb SR (2003) Regulation of epileptiform activity in hippocampus by nicotinic acetylcholine receptor activation. Epilepsy Res 56:51–65.

Shahbazian M, Young J, Yuva-Paylor L, Spencer C, Antalffy B, Noebels J, Armstrong D, Paylor R, Zoghbi H (2002) Mice with truncated MeCP2 recapitulate many Rett syndrome features and display hyperacetylation of histone H3. Neuron 35: 243–254.

Steffenburg U, Hagberg G, Hagberg B (2001) Epilepsy in a representative series of Rett syndrome. Acta Paediatr 90:34–39.

Traub RD, Jefferys JG (1994) Are there unifying principles underlying the generation of epileptic afterdischarges in vitro? Prog Brain Res 102:383–394.

Traub RD, Spruston N, Soltesz I, Konnerth A, Whittington MA, Jefferys GR (1998) Gamma-frequency oscillations: a neuronal population phenomenon, regulated by synaptic and intrinsic cellular processes, and inducing synaptic plasticity. Prog Neurobiol 55:563–575.

Uhlhaas PJ, Pipa G, Neuenschwander S, Wibral M, Singer W (2011) A new look at gamma? High- (> 60 Hz) gamma-band activity in cortical networks: function, mechanisms and impairment. Prog Biophys Mol Biol 105:14–28.

Weng SM, McLeod F, Bailey ME, Cobb SR (2011) Synaptic plasticity deficits in an experimental model of Rett syndrome: long term potentiation saturation and its pharmacological reversal. Neuroscience 180:314–321.

Whittington MA, Cunningham MO, LeBeau FE, Racca C, Traub RD (2011) Multiple origins of the cortical gamma rhythm. Dev Neurobiol 71:92–106.

Wood L, Gray NW, Zhou Z, Greenberg ME, Shepherd GM (2009) Synaptic circuit abnormalities of motor-frontal layer 2/3 pyramidal neurons in an RNA interference model of methyl-CpG-binding protein 2 deficiency. J Neurosci 29:12440–12448.

Zhang L, He J, Jugloff DG, Eubanks JH (2008) The MeCP2-null mouse hippocampus displays altered basal inhibitory rhythms and is prone to hyperexcitability. Hippocampus 18:294–309.

Zhang ZW, Zak JD, Liu H (2010) MeCP2 is required for normal development of GABAergic circuits in the thalamus. J Neurophysiol 103:2470–2481.

(Accepted 30 November 2012)
(Available online 10 December 2012)